FLORE
Repository istituzionale dell'Università degli Studi di Firenze

Spectroscopic and Potentiometric Study of the SOD Mimic System Copper(II)/acetyl-L-histidylglycyl-L-histidylglycine

Questa è la Versione finale referata (Post print/Accepted manuscript) della seguente pubblicazione:

Original Citation:

Spectroscopic and Potentiometric Study of the SOD Mimic System Copper(II)/acetyl-L-histidylglycyl-L-histidylglycine / CASOLARO M., CHELLI M., GINANNESCHI M., LASCHI F., L. MESSORI, MUNIZ-MIRANDA M., PAPINI A.M., KOWALIK-JANKOWSKA T., KOZLOWSKI H. - In: JOURNAL OF INORGANIC BIOCHEMISTRY. - ISSN 0162-0134. - STAMPA. - 89(3-4):(2002), pp. 181-190. [10.1016/S0162-0134(02)00365-3]

Availability:

The webpage https://hdl.handle.net/2158/216980 of the repository was last updated on 2026-06-14T13:17:43Z

Published version:

DOI: 10.1016/S0162-0134(02)00365-3

Terms of use:

Open Access

La pubblicazione è resa disponibile sotto le norme e i termini della licenza di deposito, secondo quanto stabilito dalla Policy per l'accesso aperto dell'Università degli Studi di Firenze (https://www.sba.unifi.it/upload/policy-oa-2016-1.pdf)

Publisher copyright claim:

Conformità alle politiche dell'editore / Compliance to publisher's policies

Questa versione della pubblicazione è conforme a quanto richiesto dalle politiche dell'editore in materia di copyright.

This version of the publication conforms to the publisher's copyright policies.

La data sopra indicata si riferisce all'ultimo aggiornamento della scheda del Repository FloRe - The above-mentioned date refers to the last update of the record in the Institutional Repository FloRe

(Article begins on next page)

07 October 2026

ELSEVIER

Journal of Inorganic Biochemistry 89 (2002) 181–190

JOURNAL OF Inorganic Biochemistry

www.elsevier.com/locate/jinorgbio

Spectroscopic and potentiometric study of the SOD mimic system copper(II)/acetyl-L-histidylglycyl-L-histidylglycine

Mario Casolaro[a], Mario Chelli[b], Mauro Ginanneschi[b,*], Franco Laschi[a], Luigi Messori[c], Maurizio Muniz-Miranda[c], Anna M. Papini[b], T. Kowalik-Jankowska[d], Henryk Kozłowski[d]

[a]*Dipartimento di Chimica and Istituto di Chimica dei Composti Organo Metallici del C.N.R., Università di Siena, Pian dei Mantellini 44, I-53100 Siena, Italy*

[b]*Dipartimento di Chimica Organica «Ugo Schiff» and Istituto di Chimica dei Composti Organo Metallici del C.N.R., Università di Firenze, Polo Scientifico Universitario, I-50019 Sesto Fiorentino (FI), Italy*

[c]*Dipartimento di Chimica, Università di Firenze, Polo Scientifico Universitario, I-50019 Sesto Fiorentino (FI), Italy*

[d]*Faculty of Chemistry, University of Wroclaw, F. Joliot-Curie 14, 50-383 Wroclaw, Poland*

Received 19 June 2001; received in revised form 3 January 2002; accepted 7 January 2002

Abstract

Stoichiometry, stability constants and solution structures of the copper(II) complexes of the *N*-acetylated tetrapeptide HisGlyHisGly were determined in aqueous solution in the pH range 2–11. The potentiometric and spectroscopic data (UV–Vis, CD, EPR and Raman scattering) show that acetylation of the amino terminal group induces drastic changes in the coordination properties of AcHGHG compared to HGHG. The N^3 atoms of the histidine side chains are the first anchoring sites of the copper(II) ion. At pH 4.7 and 5.6 both the imidazole rings cooperate in the formation of a 2N equatorial set, while, at higher pH values, 3N and 4N complexes are formed through the coordination of peptide N^- atoms. The log β values of the copper complexes of AcHGHG are by far lower than those of the corresponding species in the parent Cu^{II}–HGHG system. © 2002 Elsevier Science Inc. All rights reserved.

Keywords: Copper complexes; His-containing peptides; Tetrapeptides; EPR, Raman, UV-Vis and CD spectra; SOD activity mimics

1. Introduction

Peptide complexes with transition metals are currently widely studied for their mimic properties of the corresponding metal centres of metalloproteins. In particular, complexation by histidyl residues is found in several enzymes and transport proteins [1–5]. Thus, the structures of histidine containing peptides as well as their biological properties have been widely investigated [6] and especially their Cu^{II} complexes are largely studied. In particular, copper(II) complexes of linear and cyclic di-, tri-, tetra-, penta- and hexa-peptides were extensively examined in order to clarify the binding modes of the histidine residues located at different positions of the peptide chains [7–22]. Indeed, copper complexes of histidine-containing small peptides have a striking interest as mimicking of SOD activity [23,24], and as enzyme activating systems [25]. The same coordination compounds are considered models for studying the biological activity of proteins involved in fatal disorders like the Alzheimer's disease [26] or prion infection [27]. We have recently prepared linear and cyclic oligopeptides with an high degree of flexibility by alternating residues of histidine and glycine in the backbone [18]. The complexation properties of two of them with paramagnetic ions were investigated [19,28]. In particular we elucidated the copper complexes structures of the tetrapeptide HGHG in aqueous solution by spectroscopic and potentiometric methods. The whole experimental data revealed the ability of this small peptide to form 1:1 complexes with four N in the equatorial plane starting from acidic pH values [28]. Pharmacological studies, carried out in vitro and in vivo, on the antioxidant properties of copper complexes of both the free and the *N*-acetylated HGHG revealed that this latter compound was markedly more active, in vitro, against NBT reduction exerted by O_2^- in the xanthine/xanthine oxidase system [29]. The present paper reports extensive studies performed by potentiometric and spectroscopic methods in order to clarify the stoichiometry and the structure of the

*Corresponding author. Fax: +39-055-4573531.

E-mail address: mauro.ginanneschi@unifi.it (M. Ginanneschi).

0162-0134/02/$ – see front matter © 2002 Elsevier Science Inc. All rights reserved.
PII: S0162-0134(02)00365-3

species formed in aqueous solution within a wide range of pH values by the Cu^{II}–AcHGHG system.

2. Experimental section

N-acetyl-L-histidylglycyl-L-histidylglycine methyl ester (AcHGHGMe) was prepared following the same azide method used for the synthesis of the parent HGHGMe [18], as this method does not require imidazole protection. The hydrolysis of the pure AcHGHGMe (obtained by slow crystallization from MeOH) to *N*-acetyl-L-histidylglycyl-L-histidylglycine sodium salt, used for the spectroscopic measurements, was performed by leaving to stand for 2 days a solution of the methyl ester in aqueous methanol at about pH 9. The precipitate was collected, washed with MeOH and dried (yield: 66%): m.p. 198 °C (dec); ν_{max} (KBr pellet) 3434 (imidazole NH), 3371 (CH_3CONH), 3280 (amide NH), 1656 (amide I), 1566 cm^{-1} (amide II); δ_H (CD_3SOCD_3), 8.33 and 8.25 (3H, His^1 NH and 2×Gly NH), 7.64 and 7.59 (singlets, 2H, 2×His 2-H), 6.83 (overlapped, 2H, 2×His 5-H), 4.51–4.36 (2H, 2×His α-H), 3.85–3.59 (doublets, 4H, Gly α-H), 3.05–2.73 (4H, 2×His β-H_2), 1.82 (3H, CH_3CO); MS (FAB): 471 $(M+1)^+$. (Found: C, 43.37; H, 5.29; N, 22.67%. $C_{18}H_{24}N_8O_6Na\cdot1.5H_2O$ requires C, 43.46; H, 5.27; N, 22.53%).

2.1. Potentiometric measurements

The potentiometric apparatus has been previously described [30]. Titrations were performed at a constant temperature (25 °C) in 0.1 M NaCl with a digital PHM-84 Radiometer potentiometer, equipped with a pHG211 High pH Glass Electrode and a Ref201 Reference Electrode, and a Metrohm Multidosimat apparatus connected to computerised e.m.f. readings (mV), in relation to the volume (ml), of the added titrant. A weighed quantity (0.1–0.2 mmol) of the ester was dissolved in the glass cell containing ca. 100 ml of 0.1 M NaCl, under magnetic stirring. Forward and back-titrations were carried out with standardized HCl (0.1 M) and NaOH (0.1 M) solutions, respectively, under a presaturated nitrogen stream flowing over the surface of the solution to avoid contamination of CO_2 from the outside atmosphere. In alkaline conditions the hydrolysis reaction took place. This was confirmed by the equivalent decrease of hydroxide ions when the further back-titration with HCl was performed on the hydrolyzed compound. At least three replicates in both forward and backward titrations confirmed a good agreement with reliable results.

The complexation study with copper(II) ions was performed in a similar manner by using three different ligand-to-metal molar ratios (1:1, 2:1 and 3:1). The analytical data were processed along with potentiometric data by the program Superquad [31] on an Apple Macintosh LCII. This allowed the evaluation of the basicity and stability constants in the different experimental conditions.

2.2. Spectroscopic measurements and calculations

Temperature dependent X-band EPR spectra were recorded with a Bruker ER 200D-SRC spectrometer. The operational frequency (9.44 GHz) was tested with a Hewlett-Packard X5-32 B wavemeter and the corresponding magnetic field H was calibrated by using a DPPH solid state sample as field marker ($g_{DPPH}=2.0036$). The relevant cupric solutions frozen spectra were recorded at 100 K by suitably using the flow of the liquid nitrogen ($T=77$ K) cold vapour for cooling the X band resonance cavity. Visible absorption data were recorded at room temperature on a Shimadzu 1601PC spectrophotometer and CD spectra on a Jasco J600 spectropolarimeter. Raman spectra were registered using the exciting lines of an Argon laser, a Jobin-Yvon HG-25 monochromator, an RCA-C31034A cooled photomultiplier and a data processing system.

Semi-empirical calculations were performed using the software Spartan version 5.1.1 (Wavefunction, Inc., Irvine, CA, USA) running on a Silicon Graphics O2 workstation. The geometries were optimized using the PM3 (tm) method with transition-metals parameterization.

3. Results

3.1. Potentiometric studies

3.1.1. Basicity constants

The basicity constants ($\log K$) of the tetrapeptides AcHGHGMe and AcHGHG were evaluated by potentiometric analysis of the corresponding titration curves obtained at 25 °C and 0.1 M NaCl (Table 1). It was evident that the forward and back-titration of the methyl ester with standard solutions of NaOH and HCl, respectively, displayed a hysteresis loop, due to the hydrolysis reaction in the alkaline region attributed to the esterified carboxyl group. The results of the Superquad program showed a good fit between experimental and computed curves if only two and three basicity constants, respectively, were considered for esterified and free acyl tetrapeptides. The $\log K$ values reported in Table 2 allowed a like attribution of the protonation sites. Unlike the lowest value of $\log K_3$ for AcHGHG attributed to the carboxylate group, both $\log K_1$ and $\log K_2$ of AcHGHG and AcHGHGMe lie in the range of basicity of the imidazole ring. The former compound shows greater values due to the negatively charged carboxyl group that causes electrostatic interactions through space. This is in accordance with literature data [32,33] and with the results previously reported by us [28] on the parent HGHG peptide. The free,

Table 1
Basicity constants of the esterified and hydrolyzed tetrapeptide and comparable peptides at 298 K and 0.1 M NaCl

Peptide	log β				log K				
	HL	H_2L	H_3L	H_4L	NH_2–Lys	NH_2–Lys	N–Im	N–Im	COO^-
Ac–HGHG–OMe	6.564(8)	12.430(7)					6.56	5.87	
Ac–HGHG	6.945(9)	13.264(8)	16.51(1)				6.94	6.32	3.24
Ac–GGH[a]	7.18	10.26					7.18		3.08
Ac–EVHHQK–NH_2 [b]	10.39	17.21	23.15	27.07	10.39		6.82	5.94	3.92
Ac–EVRHQK–NH_2 [b]	10.19	16.45	20.49		10.19		6.26		4.04
Ac–AKRHRK–NH_2 [c]	11.03	20.90	27.03		11.03	9.87	6.13		
c(DD)-bisHim[d]	7.28	13.82					7.28	6.54	
c(EE)-bisHim[d]	7.17	13.76					7.17	6.58	

Values in parentheses are standard deviations.
[a] Ref. [41].
[b] Ref. [26].
[c] Ref. [42].
[d] Ref. [23].

protonable, primary amino group, of the tetrapeptide HGHG strongly suppressed the basicity of the neighboring imidazole N^3. In the *N*-acetylated derivative, the closer imidazole log *K* increased of about 1 unit (6.32 in AcHGHG, 5.33 in HGHG), while a lower increasing pattern was observed for the other imidazole ring (6.94 in AcHGHG, 6.54 in HGHG).

On the basis of these results we can reasonably attribute the first protonation step of both forms of the ligand molecule to the imidazole nitrogen close to the carboxyl group.

3.1.2. Stability constants

The stability of the Cu^{II}–AcHGHG (CuHL) system was evaluated by potentiometric analysis at 25 °C in 0.1 M NaCl and with three different ligand/metal(II) molar ratios (1:1, 2:1 and 3:1). To fit potentiometric data by the Superquad program, different species were considered and the best model refined the five species $CuHL^{2+}$, CuL^+, $CuH_{-1}L$, $CuH_{-2}L^-$ and $CuH_{-3}L^{2-}$.

The stability constants (log β), reported in Table 2, were used together with log *K* values to compute the species distribution curves (Fig. 1).

3.2. X-band EPR

Due to the electronic nature of the copper(II) (electronic ground state ^2E_g), in the presence of significant tetragonal elongation of the O_h original coordination sphere the $S=1/2$ unpaired electron is mainly located in the cupric $3d_{x^2-y^2}$ AO [34]. The temperature and pH dependent X-band EPR lineshape analysis characterizes magnetic and structural features of the Cu^{II}–AcHGHG complexes on the basis of the $S=1/2$ Electron Spin Hamiltonian, which accounts for the Zeeman electron interaction ($g\beta HS$) modulated by the cupric hyperfine interaction (*AIS*) and the subsequent nitrogen superhyperfine interaction ($\Sigma_i A_i I_i S$). As a function of the experimental conditions different cupric species are identified and the corresponding geometries, particularly the equatorial ligand atoms donor set and the relevant charge, can be proposed.

Fig. 2 shows the X-band EPR spectra of the Cu^{II}–AcHGHG complexes at different pH values at room temperature (RT) and in Table 3 the relevant paramagnetic parameters are collected. The EPR lineshapes of the cupric complexes (Fig. 2) were investigated referring to the maxima in the plot of the Cu^{II}–AcHGHG complex species distribution (Fig. 1). By comparison, in the ''pure'' RT Cu^{II}–H_2O spectrum (pH 2.3; $g_{iso}>g_{electron}=2.0023$) [34,35] the overall linewidth overlaps the four isotropic cupric hpf splittings [I-Cu(63,65)=3/2] in an unique unresolved signal [$g_{averaged}$(298 K)=2.190(5), $\Delta H_{averaged}$(298 K)=150(5)G], while the liquid nitrogen temperature (LN) spectrum ($g_{\parallel}>g_{\perp}>g_{electron}$; $\langle g\rangle > g_{electron}$) displays axial structure with hpf cupric resolution of the $g_{\parallel}$ region. Adding the tetrapeptide to the cupric solution (metal-to-ligand molar ratio=1:1) noticeably changes both the RT and LN lineshapes, exhibiting EPR parameters typical of significant interaction copper(II)-ligand while the pH decreases to 1.9. Raising the pH at 2.9, the cupric solution displays evolution of the LN and RT lineshapes, suggesting changes of the coordination mode of Cu^{II}–AcHGHG complex. As a tentative hypothesis the pH 1.9 spectra could be assigned to an ''outer sphere'' coordination [(Cu^{II}–H_2O)–AcHGHG], being the ligand located in the second coordination sphere (dipolar interaction), while at pH 2.9 the actual spectra could be explained assuming the direct binding of the tetrapeptide with the Cu^{II} (CuHL species). Taking into account the Blumberg–Peisach approach [36] the $f=g_{\parallel}/A_{\parallel}$ ratio (f= tetragonal distortion factor) could be interpreted assuming an equatorial ligand interaction via the $-COO^-$ residue (four O atoms in the planar donor set with corresponding charge of +1). The RT spectra (Fig. 2a,b) refer to the above species, the upper ones relevant to the first derivative mode, the lower ones to the second derivative mode.

Raising pH induces important variations on the cupric EPR features; particularly, in the pH range of 4.5–7.0 the

Table 2
Stability constants of copper(II) complexes of Ac–HGHG (concentration constants at 298 K and 0.1 M NaCl) and comparable peptides

Peptide	log β					
	CuH_2L	CuHL	CuL	$CuH_{-1}L$	$CuH_{-2}L$	$CuH_{-3}L$
Ac–HGHG		11.04(10)	6.49(3)	0.40(4)	−6.13(4)	−16.41(5)
Ac–GGH[a]			4.24	−2.26	−9.61	−18.86
Ac–EVHHQK–NH_2 [b]	21.03	16.21	10.18	2.86	−6.31	−16.72
Ac–EVRHQK–NH_2 [b]		14.01		1.93	−6.66	−16.83
Ac–AKRHRK–NH_2 [c]	23.70		12.45	3.98	−5.94	−16.92
c(DD)-bisHim[d]		11.09	6.65	−0.28	−8.39	
c(EE)-bisHim[d]		10.97	6.49	−0.40	−8.79	
	log K^* [e]					
	1N (N_{Im})	2N (N_{Im}, N^-)	3N ($2N_{Im}$, N^-)	3N (N_{Im}, $2N^-$)	4N ($2N_{Im}$, $2N^-$)	4N (N_{Im}, $3N^-$)
Ac–HGHG	−2.22	−6.54	−12.86	−13.07	−19.39	−23.35
Ac–GGH[a]	−2.94	−9.44		−16.79		−26.04
Ac–EVHHQK–NH_2	−2.12	−7.03	−12.97	−14.35		−23.52
Ac–EVRHQK–NH_2	−2.44			−14.52		−23.11
Ac–AKRHRK–NH_2	−3.33			−14.58		−23.05
c(DD)-bisHim	−2.73	−7.56	−14.10	−15.67	−22.21	
(EE)-bisHim	−2.79	−7.57	−14.16	−15.96	−22.55	
	Values for ionization of the first, second and third amide groups					
	pK_1 (amide)		pK_2 (amide)		pK_3 (amide)	
Ac–HGHG	6.09		6.53		10.28	
Ac–GGH	6.50		7.35		9.25	
Ac–EVHHQK–NH_2	6.03		7.32		9.17	
Ac–EVRHQK–NH_2					8.59	
Ac–AKRHRK–NH_2					8.47	
c(DD)-bisHim	6.93		8.11			
c(EE)-bisHim	6.89		8.39			

[a,b,c,d]Refs. as in Table 1. [e] log K^* = log $\beta(CuH_jL)$ − log $\beta(H_nL)$ [H_2L with Ac–EVRHQK–NH_2, Ac–GGH; H_3L with Ac–AKRHRK–NH_2 and Ac–EVHHQK–NH_2 for CuH_2L but H_2L for CuL, $CuH_{-1}L$ and $CuH_{-2}L$ species; H_2L or HL with Ac–HGHG and *c*(DD)-bisHim and *c*(EE)-bisHim].

RT and LN signals indicate the contemporary presence of different cupric species (CuHL, CuL, $CuH_{-1}L$ complexes) in accordance with the plot of Fig. 1. Here, at pH 4.7, the CuHL species is not EPR detectable due to the overlapping of the previous cupric complexes, predominant in this experimental condition. At pH 5.5 the major complex is the CuL; the Blumberg–Peisach analysis assigns it to 2N2O equatorial coordination set, with a corresponding charge of +1. There are no shpf resolutions for this complex, due to the actual ΔH_i largely overlapping the underlying N signals. Accordingly, the present EPR parameters allow us to evaluate an upper limit for such an shpf interactions, as $A_i(N) \leq \Delta H_i/4$. Again raising the pH,

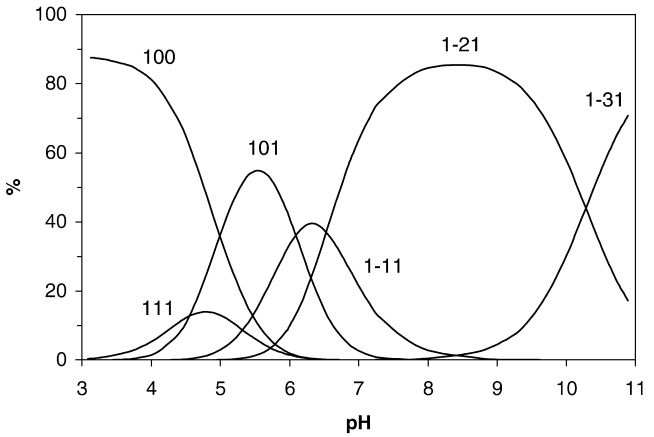

Fig. 1. Computed species distribution curves for the Cu^{II}–HGHG system (ligand-to-metal ratio 1:1) at 25 °C in 0.1 M NaCl. Each species $M_pH_qL_r$ is indicated by subscripts p, q and r.

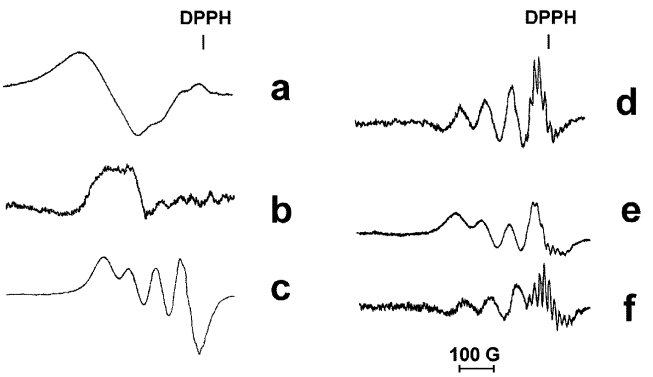

Fig. 2. X-band EPR spectra of the Cu^{II}–AcHGHG system (ligand-to-metal ratio = 1:1) at RT. pH = 2.9: (a) first derivative, (b) second derivative. pH = 8.4: (c) first derivative, (d) second derivative. pH = 10: (e) first derivative, (f) second derivative.

Table 3
Temperature and pH dependent X-band EPR parameters of the Cu^{II}–AcHGHG system (ligand-to-metal ratio = 1:1)

pH	g_{iso}	$g_{\parallel}$	$g_{\perp}$	ΔH_{iso}	$\langle g \rangle^a$	A_{iso}	$A_{\parallel}$	$A_{\perp}$	$A_{\perp}$(N)	$\langle A \rangle^a$	A_{iso}(N)
2.3[b]	2.190	2.421	2.091	150G	2.201	≤5.1	15.8	≤2.1	–	≤6.5	–
1.9	2.178	2.377	2.073	155G	2.174	≤5.3	13.3	≤2.4	–	≤6.4	–
2.9	2.170	2.364	2.065	160G	2.165	≤5.4	16.9	≤2.9	–	≤7.4	–
5.5	2.149	2.292	2.051		2.131	≤6.5	17.2	≤2.5	≤0.6	≤6.8	≤1.1
7.0–10.0	2.106	2.250	2.039		2.109	7.2	18.3	≤2.7	0.8	≤8.2	1.1
≥10.8	2.096	2.200	2.045		2.097	8.3	19.7	≤3.2	≤1.2	≤8.4	1.5

$[Cu^{2+}] = 1 \times 10^{-3}$M; A_i: $\pm 0.6 \times 10^{-3}$ cm^{-1}; g_i: ±0.006.
[a] Values evaluated from the formulae: $\langle g \rangle = 1/3(g_{\parallel} + 2g_{\perp})$, $\langle A \rangle = 1/3(A_{\parallel} + 2A_{\perp})$.
[b] Cu^{II}–H_2O system.

at pH 6.5 the minor $CuH_{-1}L$ species is EPR undetectable due to the presence of both the previous CuHL and the new $CuH_{-2}L$ complexes.

From neutral pH to 11, the $CuH_{-2}L$ cupric species and the new $CuH_{-3}L$ complex are in equilibrium; in particular, at pH 8.4 the $CuH_{-2}L$ species is predominant (Fig. 2c,d). The RT spectrum displays a resolved shpf structure in the cupric $m_I = +1/2$ and $+3/2$ lines, while the corresponding LN spectrum exhibits partial shpf resolution in the top of the $g_{\perp}$ region. Moreover, the RT spectrum exhibits a significant m_I(Cu) dependence of the hpf splittings and a noticeable $\Delta H_{isotropic}$ variation, particularly on the fourth hpf absorption. This spectral behaviour is typical of large and unsymmetrical cupric species and underlines the importance of the original g_i and A_i structural anisotropies not completely averaged in fast motion conditions [34,36]. The actual RT septuplet testifies for the magnetic interaction of the unpaired electron with three equatorially bound nitrogen atoms (3NO atom donor set), with an equatorial charge intermediate between 0 and -1. Values of pH higher than 10 induce further changes in the cupric lineshapes, as shown in Fig. 2e,f. Here, the $CuH_{-3}L$ species is now identified in the RT spectrum, being its $m_I = +3/2$ high field line partially overlapped to that of the previous $CuH_{-2}L$ species. Accordingly, the relevant LN spectrum is broadened due to the presence of both the $CuH_{-2}L$ and $CuH_{-3}L$ signals. The isotropic parameters of the $CuH_{-3}L$ nonuplet suggest the occurrence of a slightly larger nitrogen shpf splitting, due to the interaction of the $S = 1/2$ electron with four nearly equivalent nitrogens equatorially positioned. Correspondingly, the Blumberg–Peisach approach indicates an equatorial charge of -1. Getting back to the previous acidic conditions the overall spectral sequence displays complete reversibility of the total chemical equilibrium. Temperature dependent X-band EPR measurements carried out at lower metal-to-ligand molar ratios (from 1:2 to 1:5) and pH range 3–10 do not show significant variations on the corresponding lineshapes; correspondingly, higher metal-to-ligand molar ratios (1.5:1, 2:1), under the same experimental conditions, account for the presence of the previous cupric complexes in the presence of the free copper(II)–H_2O species.

3.3. Raman spectra

Raman studies of the cupric complexes of AcHGHG can offer useful information for identifying the type of bonds with the metal ion and the different interaction sites of the ligand. The same approach was employed for the parent tetrapeptide HGHG [28]. As in the case of HGHG, the variations of the Raman spectra of AcHGHG in aqueous solution, at different pH values, are related to the formation of different complexes with the chelated ion.

A spectral analysis of these complexes, however, needs a correct assignment of the Raman bands observed for the free ligand. The strongest Raman bands of the free ligand HL can be attributed to the histidine residue, as already observed for the non-acetylated compound. A comparison between the strongest Raman bands of AcHGHG and His with the predominant attribution [37] is proposed in Table 4; the Raman spectra of the free ligand are reported in Fig. 3. Concerning the peptide backbone, the Raman bands observed with medium intensities at 1030–1050 cm^{-1} are assigned to C–N stretchings of the peptide bonds. The amide III band occurs at ca. 1270 cm^{-1}, overlapped by the strong C–H bending vibration of the histidine residue. The amide I band is observed at ca. 1650 cm^{-1} as a weak shoulder of the histidine band at ca. 1630 cm^{-1}. The band observed in alkaline medium at ca. 1395 cm^{-1} is attributed to the symmetric stretching mode of the carboxylate group.

The Raman bands of the Cu^{II}–AcHGHG coordination compounds undergo marked variations in aqueous solution at different pH values (Fig. 4). In order to correctly compare the Raman spectra of the different complexes, the SO_4^{2-} ion vibration at ca. 980 cm^{-1} has been chosen as the reference. At pH 2 the ligand does not interact with the metal ion, because the Raman spectrum closely resembles that of the free peptide. The occurrence of the asymmetric stretching mode of the bonded carboxylate at ca. 1595 cm^{-1}, together with the symmetric stretching band at ca. 1370 cm^{-1}, shows interaction of this group with Cu^{II} ion. These bands could be clearly detected from pH 4.75 to 6.5. At alkaline pH values the nitrogen atoms, belonging to the histidine residues as well as to the peptide bonds, are involved in coordination with the copper ion. Indeed, the

Table 4
Raman bands of AcHGHG and His at different pH

pH 3		pH 8.7		Assignment
Ac–HGHG	His	Ac–HGHG	His	
994	992	990	992	Ring deformation
1194	1196			″
		1236	1236	″
1270	1270	1274	1268	Ring CH bending
			1286	Ring stretching
1326	1334	1322	1324	Ring breathing
1440	1440	1440	1440	CH_2 bending
1489	1490	1490	1494	Ring stretching + ring CH bending
		1578	1572	Ring stretching
1629	1630			″

occurrence of the band at 1585 cm^{-1} is related to the ring stretching of metal-bound histidine [38]. Moreover, the peak observed at about 1405 cm^{-1} can be attributed to the deprotonation of amide nitrogens through the binding of Cu^{II}. This matches what is proposed for the 1420 cm^{-1} band observed in aqueous alkaline medium in the case of other oligopeptides including histidine and glycine residues [39]. In particular, at pH 8.4 the interaction of two imidazole rings and two peptide nitrogens can be proposed. At pH 12 the intensification of the peptide C–N stretching modes suggests that a third nitrogen atom of the backbone can be involved in the coordination with Cu^{II}. Finally, in a weakly acidic medium, at pH 5.5–6.5, it is possible an interaction of, at least, one imidazole ring with Cu^{II}, due to the decreasing intensities of the imidazolium bands at ca. 1190 and ca. 1490 cm^{-1}. Until pH ca. 6.5 the two histidine imidazoles of the free ligand are predominantly protonated; hence, this spectral evidence can be reasonably attributed to coordination of the histidine residue, resulting in deprotonation of the imidazolium ring.

3.4. Visible and CD spectra

Visible optical spectra were obtained for solutions containing ligand-to-metal ratio 1:1 and 2:1, and for concentrations varying from 5×10^{-3} to 2×10^{-2} M. The spectra are characterized by a broad d–d transition in the visible range. At pH 5.8, corresponding to the maximum of the CuL species, the visible band is centred at 660 nm with a broad shoulder at lower energies. As the pH is raised from acidic to alkaline values, an increase of the absorbance and a progressive blue shift was observed in the

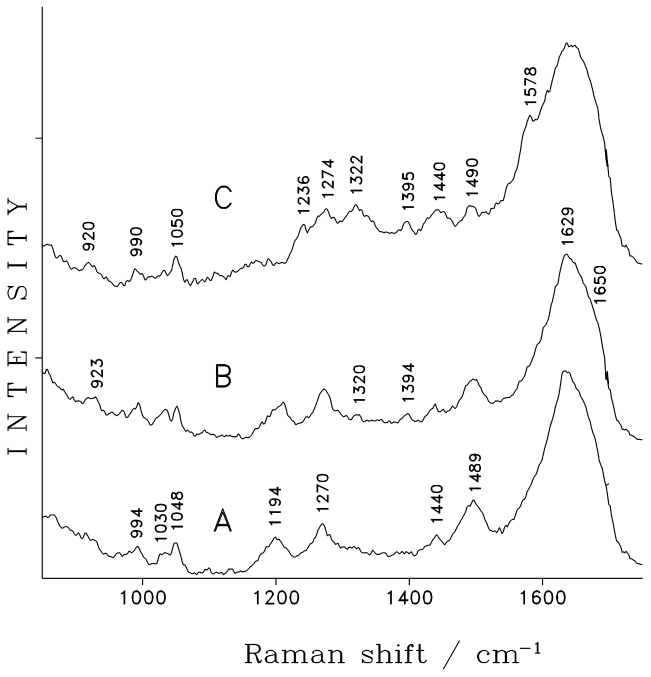

Fig. 3. Raman spectra of AcHGHG in aqueous solutions at different pH: 2.9 (A); 5.1 (B); 8.7 (C).

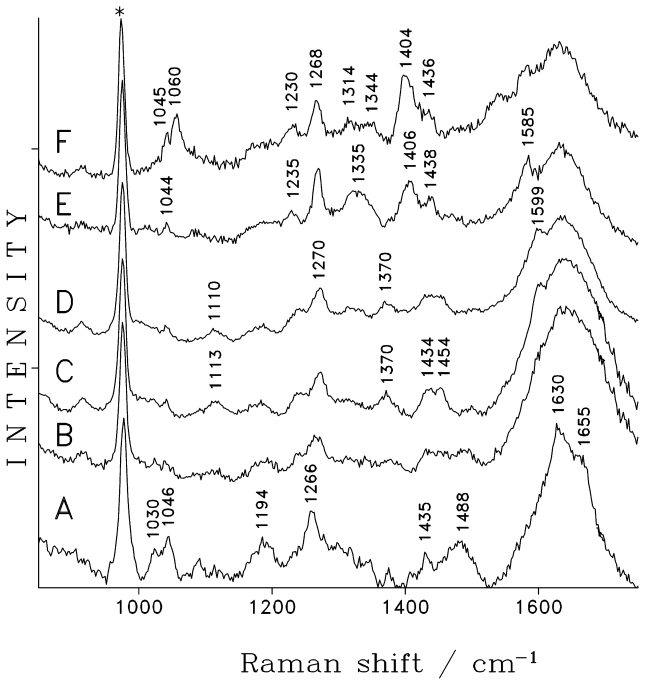

Fig. 4. Raman spectra of Cu^{II}–AcHGHG in aqueous solutions at different pH: 2.0 (A); 4.75 (B); 5.55 (C); 6.45 (D); 8.4 (E); 12.0 (F). Dotted band at ~980 cm^{-1} refers to SO_4^{2-} ion vibration.

Table 5
Spectroscopic data for copper(II) complexes of AcHGHG

Species	UV–VIS		CD	
	λ (nm)	ε (M^{-1} cm^{-1})	λ (nm)	ε (M^{-1} cm^{-1})
CuL	660[a]	38	622[a]	+0.026
			317[b]	−0.022
$CuH_{-2}L$	564[a]	119	575[a]	+0.524
			347[b]	+2.062
			301[c]	−1.799
$CuH_{-3}L$	555[a]	125	593[a]	+1.516
			477[a]	−0.645
			319[b,c]	+1.873

[a] d–d transition.
[b] $N_{Im} \rightarrow Cu^{2+}$ charge transfer transition.
[c] $N^{-}_{amide} \rightarrow Cu^{2+}$ charge transfer transition.

pH range 6–9, with no evidence of isosbestic points. At pH corresponding to the predominance of the $CuH_{-2}L$ species, the λ_{max} is located at 565 nm. Notably upon further increasing pH from 9 to 12, an additional blue shift of 10 nm is observed with evidence of an isosbestic point around 600 nm.

Parallel CD measurements were carried out on the same system. In Table 5, that shows the absorptions registered at pH values corresponding to the maximum percentage of the computed species in the distribution curves, we report the UV–vis and CD data taken at pH values corresponding to the major species. The first, well structured, CD spectrum is observed when $CuH_{-2}L$ species is formed at pH above 7. Large CD perturbations are observed in concomitance with the transition from the $CuH_{-2}L$ to the $CuH_{-3}L$ species suggesting the occurrence of an important conformational rearrangement around the copper ion.

4. Discussion

The values of ligand protonation constants are collected in Table 1. The values of the reported log K allow a like attribution of the subsequent protonation steps. At the metal-to-ligand equimolar or lower ratios (1:2, 1:3) the pH-metric titration curves account for the presence of five species for the Cu^{II}–AcHGHG system, in the pH range 3–11 (Fig. 1). No binuclear species nor bis-complexes were detected on the basis of potentiometric and spectral data. The ^{1}H NMR spectra in D_2O of the equilibrium mixture, at any pH, do not provide useful information as detectable signals arise from the basis line only when the ligand-to-copper ratio is more than 30. For such high molar ratios the coordination species may be quite different from those detected in our experimental conditions [40].

As shown by potentiometry, the CuHL and $CuH_{-1}L$ complexes are minor species and cannot be fully characterized by spectroscopic methods. However, on the basis of the EPR spectrum of Cu^{II}–AcHGHG system at pH 2.9 and of the Raman spectrum of the parent Cu^{II}–HGHG taken at pH 4.5, we could suggest that, also for CuHL complex the imidazole N^3 and $-COO^-$ groups are involved in the coordination. The experimental value of log K* (Table 2), which is higher than those obtained for histidine-containing peptides where the carboxy terminal group is not available for the coordination [26,41,42], may support this suggestion [43]. For the species CuL the CD spectrum shows a CT transition $N_{Im} \rightarrow Cu^{II}$ at 317 nm while the EPR parameters $A_{\parallel} = 17.2 \times 10^{-3}$ cm^{-1} and $g_{\parallel} = 2.292$ are consistent with $2N_{Im}$ atoms in the planar coordination; accordingly, similar values were observed for copper(II) complexes coordinated by two molecules of imidazole [44] and in the Cu^{II}–AcEVHHQK–NH_2 system [26]. The low protonation constant of the CuL species (4.5) is comparable to that of peptides with imidazole nitrogen coordination [22], suggesting that a second imidazole N^3 is involved in the bonding with the metal ion. On the other hand, the log β of this species is very close to that found for the CuL species of the Cu^{II}-*c*(DD)-bisHim and Cu^{II}-*c*(EE)-bisHim systems, containing two N_{Im} in the plane (Table 2). At pH 5.6, the species CuL is predominant but in equilibrium with four other species (Fig. 1). Tentatively, we can say that the visible spectrum ($\lambda_{max} = 660$ nm) is in accordance with the calculated λ_{max} for $2NOO'$ ($2N_{Im}$, COO^-, water) equatorial set (665 nm) [45]. At this pH, the Raman spectrum shows only a very weak signal corresponding to the imidazolium ring breathing, probably due to the small amount of the free ligand in equilibrium. The relevant calculated structure is depicted in Fig. 5a.

Increasing the pH, the $CuH_{-1}L$ complex is formed. The deprotonation constant for $CuL \leftrightarrows CuH_{-1}L + H^+$ is -6.09 and can be assigned to the coordination of deprotonated amide group (Table 2). The log K* value for the $CuH_{-1}L$ complex is close to the log K* calculated for the same species of other complexes where two N_{Im} are involved in the equatorial plane. Again, the log β constants for Cu^{II}–AcHGHG, Cu^{II}-*c*(DD)-bisHim and Cu^{II}-*c*(EE)-bisHim systems are comparable (Table 2); this strongly suggests, for our species, the presence of two N_{Im} and one peptide N^- equatorially bound. When the $CuH_{-1}L$ complex looses

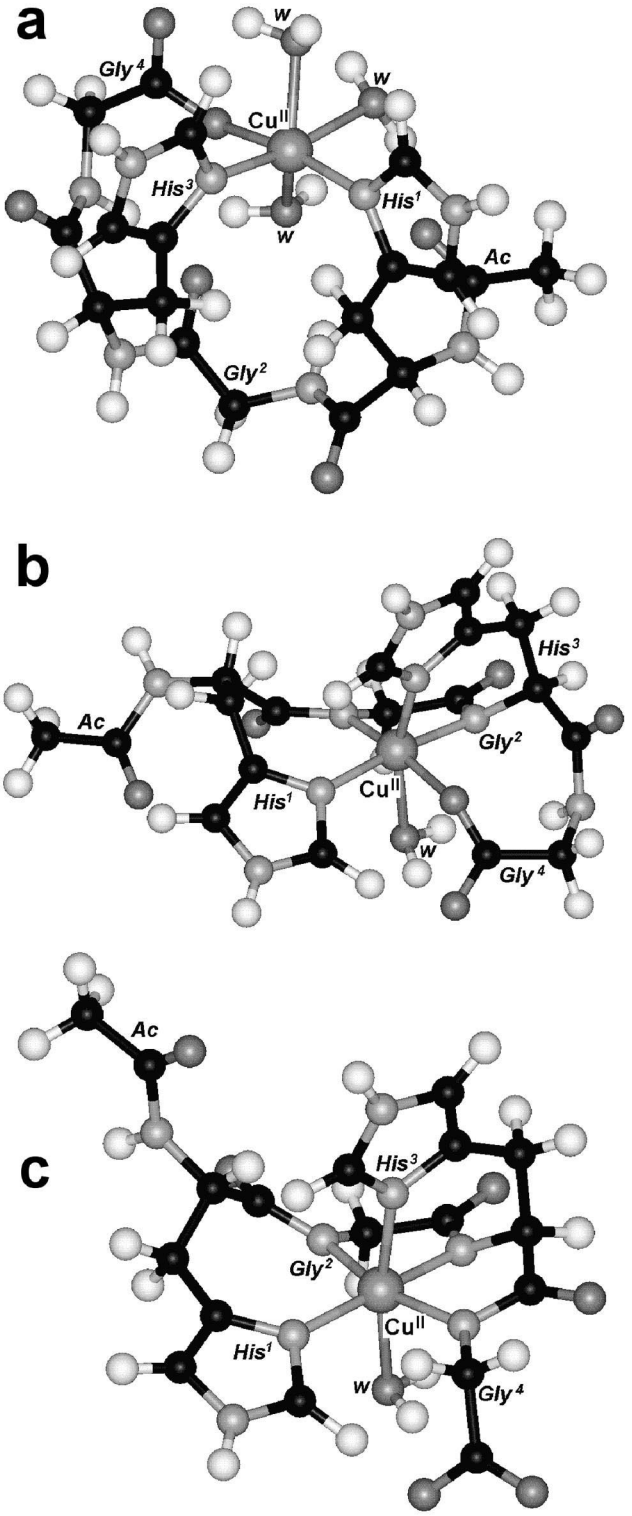

Fig. 5. Optimized structures of the main HL/Cu^{II} complexes at (a) pH 5.6, (b) pH 7.0 and (c) pH>8, obtained from PM3(tm) semi-empirical calculations.

the next proton, the $CuH_{-2}L$ species is formed, being predominant in a wide pH range (7–9) of the solution. The temperature dependent EPR line shapes indicate the presence of a 3NO donor group in the equatorial plane (Fig. 2), due to a second deprotonated peptide group in place of one N_{Im} [26,46]; this is also suggested by the blue shift of the visible spectrum (564 nm, Table 5) in accordance with the calculated λ_{max} (565 nm) for N_{Im}, $2N^{-}COO^{-}$ equatorial set. In the CD spectrum the ct transitions $N_{Im} \rightarrow Cu^{II}$ at 347 nm and $N_{amide} \rightarrow Cu^{II}$ at 301 nm are clearly detectable. Moreover, the observation of λ_{max} at 564 nm is indicative of a three or four nitrogens in-plane coordination, the $A_{\parallel}$ value reflecting some apical interaction. Bonomo and coworkers claimed, for the copper(II)–AcHGGG–NH_2 complex, in the same pH range, a planar coordination with N_{Im}, $2N^{-}$ and a water molecule, being the apical position occupied by another amide nitrogen [46]. These authors found for this species $\lambda_{max}=626$ nm; the blue shift showed by Cu^{II}–AcHGHG complex (Table 5) is probably due to the in-plane carboxylate group and to the imidazole coordination in the apical position. The EPR and Raman data did not indicate whether His^1 or His^3 is bonded in the equatorial plane. Molecular models demonstrated that His^3 nitrogen and COO^{-} group cannot cooperate together in the equatorial plane; on the other hand, the substitution of the carboxy group with a water molecule resulted in a higher value of the calculated λ_{max} (584 nm); consequently, the equatorial position of His^1 is supported only by the visible spectrum. The coordination of the third amide nitrogen occurs at higher pH values ($pK_3=10.28$, Table 2) compared to those of other N-blocked peptides containing histidine residues [26,42]. Thus, the species $CuH_{-3}L$ becomes predominant only at pH ca. 11 (Fig. 1). The EPR parameters ($A_{\parallel}=19.7\times10^{-3}$ cm^{-1}, $g_{\parallel}=2.200$) and the appearance of a nonuplet in the RT spectrum are in accordance with a 4N donor set in the equatorial plane [46]. Although the calculated equatorial charge accounts for the presence of three N^{-} amide atoms, the pH value relevant to the maximum concentration for this species could induce, in principle, the deprotonation of the pyrrole imidazole nitrogen from the previous species [47]. The $\log K^*$ (−23.35) of this copper complex is comparable to those of the ligands Ac–EVHHQK–NH_2, Ac–EVRHQK–NH_2 and Ac–AKRHRK–NH_2 (Table 2), suggesting the same coordination mode, i.e. through deprotonation of a peptide nitrogen. This hypothesis is supported by the Raman spectra which indicate the involvement of a higher number of peptide nitrogens in respect to the $CuH_{-2}L$ species. However, the hypothesis of the formation, at this pH value, of an imidazolate ion cannot be completely discarded. The Vis spectra of this species, taken at pH 11, 11.5 and 12 did not substantially differ either for the λ_{max} or for the $\log \varepsilon$. Because at this pH the concentration of the $CuH_{-2}L$ complex is negligible, we could observe that the d–d transition energy at 555 nm is significantly red shifted if compared to the maximum (523 nm), calculated for in plane 3NN′ set involving three peptide nitrogens. This shift could be due to strong apical nitrogen coordination [46], caused, in our case as for the GGGH system [22], by one imidazole residue. In a previous paper [29], we have

shown that both Cu–HGHG and Cu–AcHGHG systems decreased the rate of NBT reduction induced by superoxide ion in vitro at pH 7.4 and in phosphate buffer. Their activity was compared to suitable concentrations of copper sulphate in the same conditions. The values of IC_{50} (0.67 and 0.083 μM, respectively) indicated that the Cu–AcHGHG system is significantly more active than the parent compound. At pH 7.4 the species $CuH_{-2}L$ is largely predominant (Fig. 1); the relevant log β (−6.13) is by far lower than the corresponding complex of the Cu–HGHG system (log $\beta = -0.54$). Therefore, the former is able to release a larger amount of Cu(II) in solution. At the same time, in the unprotected peptide, this major complex is completely blocked by the peptide donors, while in the case of AcHGHG there is some free site to interact with copper ion. Both these factors could explain the greater SOD-mimic activity of the Cu–AcHGHG system.

4.1. Molecular geometry computations

In Fig. 5 are shown three lowest energy geometries relevant to the CuL, $CuH_{-2}L$ and $CuH_{-3}L$ species. These structures have been calculated taking into account the donor sets suggested by the potentiometric and spectroscopic data discussed above. In the CuL system (Fig. 5a) the two imidazole rings contribute to the 2NOO′ equatorial system, while in the $CuH_{-2}L$ species (Fig. 5b) the geometry optimization converged to an octahedral stereochemistry with the 3NO equatorial donor set formed by His imidazole, two peptide nitrogens and $-COO^-$ group. We considered that the His^1 N_{Im} is, probably, involved in the planar coordination and His^3 is the apical donor. In Fig. 5c is depicted the structure of the $CuH_{-3}L$ species with 5NO octahedral donor set, showing three backbone nitrogens and one imidazole nitrogen in the equatorial plane.

5. Conclusions

Potentiometric and spectroscopic investigations show that, in the AcHGHG unit, carrying blocked NH_2 group, the histidine side-chains act as the first Cu^{II} anchoring sites through N^3 atoms. Moreover, two imidazole rings are involved in the planar coordination up to pH 7. At higher pH the stepwise interaction of the amide groups with the copper(II) ion occurs and one of the imidazole residues is switched to the apical position. Differently from the parent HGHG compound, where, going on from pH 5, the data indicated the presence of 4N equatorial atom donor set [28], the acetylated derivative shows a gradual increase in the number of nitrogen coordination along the five species pointed out by the potentiometric data. The stability constant of the complex $CuH_{-2}L$, which is the predominant species, at physiological pH, is about six orders of magnitude lower than that of the corresponding species of HGHG, where the NH_2 group is involved in the coordination.

References

[1] D.R. Garmer, M. Krauss, J. Am. Chem. Soc. 114 (1992) 6487–6493.
[2] V.K. Yachandra, V.J. DeRose, M.J. Latimer, I. Mukerji, K. Sauer, M.P. Klein, Science 260 (1993) 675–679.
[3] I. Bertini, A. Scozzafava, in: H. Sigel (Ed.), Metal Ions in Biological Systems, Copper(II) as probe in substituted metalloproteins, Vol. 12, Marcel Dekker, New York, 1981, pp. 31–74.
[4] M.J. Ettinger, in: R. Lontie (Ed.), Copper Protein and Copper Enzymes, Vol. 3, CRC Press, Boca Raton, FL, 1984.
[5] N.D. Chasteen (Ed.), Vanadium in Biological Systems. Physiology and Biochemistry, Kluwer, Dordrecht, 1990.
[6] H. Kozłowski, W. Bal, M. Dyba, T. Kowalik-Jankowska, Coord. Chem. Rev. 184 (1999) 319–346.
[7] R.P. Bonomo, F. Bonsignore, E. Conte, G. Impellizzeri, G. Pappalardo, R. Purrello, E. Rizzarelli, J. Chem. Soc., Dalton Trans. (1993) 1295–1300.
[8] J. Ueda, M. Miyazaki, Y. Matsushima, A. Hanaki, J. Inorg. Biochem. 63 (1996) 29–39.
[9] P.G. Daniele, E. Prenesti, R. Aigotti, G. Ostacoli, J. Inorg. Biochem. 58 (1995) 139–146.
[10] W. Bal, M. Jezowska-Bojzuk, H. Kozłowski, L. Chruscinski, G. Kupryszewski, B. Witczuk, J. Inorg. Biochem. 57 (1995) 235–247.
[11] P.G. Daniele, E. Prenesti, O. Zerbinati, R. Aigotti, G. Ostacoli, Spectrochim. Acta 49A (1993) 1373–1378.
[12] K. Takahara, Y. Ide, Inorg. Chim. Acta 183 (1991) 195–202; E. Farkas, I. Sóvágó, T. Kiss, A. Gergely, J. Chem. Soc., Dalton Trans. (1984) 611–614.
[13] P.G. Daniele, O. Zerbinati, V. Zelano, G. Ostacoli, J. Chem. Soc., Dalton Trans. (1991) 2711–2715.
[14] L.D. Pettit, S. Pyburn, W. Bal, H. Koslowski, M. Bataille, J. Chem. Soc., Dalton Trans. (1990) 3565–3570.
[15] P.G. Daniele, O. Zerbinati, R. Aruga, G. Ostacoli, J. Chem. Soc., Dalton Trans. (1988) 1115–1120.
[16] J.-P. Laussac, A. Robert, R. Haran, B. Sarkar, Inorg. Chem. 25 (1986) 2760–2765.
[17] S. Goldestein, G. Czapski, D. Meyerstein, J. Am. Chem. Soc. 112 (1990) 6489–6492.
[18] M. Chelli, M. Ginanneschi, A.M. Papini, D. Pinzani, G. Rapi, E. Borghi, F. Laschi, M. Occhiuzzi, J. Chem. Res. (S) (1993) 437; (M) 2928–2936.
[19] E. Borghi, F. Laschi, M. Occhiuzzi, M. Chelli, M. Ginanneschi, A.M. Papini, G. Raphi, J. Chem. Res. (S) (1994) 48–49.
[20] J. Ueda, N. Ikota, A. Hanaki, K. Koga, Inorg. Chem. Acta 135 (1987) 43–46.
[21] I. Sóvágó, D. Sanna, A. Dessì, K. Várnagy, G. Micera, J. Inorg. Biochem. 63 (1996) 99–117.
[22] K. Várnagy, J. Szabó, I. Sóvágó, G. Malandrinos, N. Hadjiliadis, D. Sanna, G. Micera, J. Chem. Soc., Dalton Trans. (2000) 467–472.
[23] R. Bonomo, E. Conte, G. Impellizzeri, G. Pappalardo, R. Purrello, E. Rizzarelli, J. Chem. Soc., Dalton Trans. (1996) 3093–3099.
[24] R. Pogni, M.C. Baratto, E. Busi, R. Basosi, J. Inorg. Biochem. 73 (1999) 157–165.
[25] T. Kowalik-Jankowska, M. Jasionowski, L. Lankiewicz, J. Inorg. Biochem. 76 (1999) 63–70.
[26] T. Kowalik-Jankowska, M. Ruta-Dolejsz, K. Wisniewska, L. Lankiewicz, H. Kozłowski, J. Chem. Soc., Dalton Trans. (2000) 4511–4519.
[27] E. Aronoff-Spencer, C.S. Burns, N.I. Avdievich, G.J. Gerfen, J.

Peisach, W.E. Antholine, H.L. Ball, F.E. Cohen, S.B. Prusiner, G.L. Millhauser, Biochemistry 39 (2000) 13760–13771.
[28] M. Casolaro, M. Chelli, M. Ginanneschi, F. Laschi, M. Muniz-Miranda, A.M. Papini, G. Sbrana, Spectrochim. Acta 55A (1999) 1675–1689.
[29] M. Ciuffi, C. Cellai, S. Franchi-Micheli, P. Failli, L. Zilletti, M. Ginanneschi, M. Chelli, A.M. Papini, F. Paoletti, Pharmacol. Res. 38 (1998) 279–287.
[30] M. Casolaro, F. Bignotti, P. Ferruti, J. Chem. Soc., Faraday Trans. 93 (1997) 3663–3668.
[31] P. Gans, A. Sabatini, A. Vacca, J. Chem. Soc., Dalton Trans. (1985) 1195–1200.
[32] R.I. Shrager, J.S. Cohen, S.R. Heller, D.H. Sachs, A.N. Schechter, Biochemistry 11 (1972) 541–547.
[33] M. Tanokura, M. Tasumi, T. Miyazawa, Biopolymers 15 (1976) 393–401.
[34] F.E. Mabbs, D. Collins, Studies in Inorganic Chemistry, Electron Paramagnetic Resonance of d-Transition Metal Compounds, Vol. 12, Elsevier, Amsterdam, 1992.
[35] ESRMGR Simulation Program, by G. DellaLunga, Chemistry Department of Siena, 1995, pp. 1–10;
G.P. Lozos, B.M. Hoffman, C.G. Franz, QCPE 11 (1974) 265.
[36] J. Peisach, W.E. Blumberg, Arch. Biochem. Biophys. 165 (1974) 691–708.
[37] S. Martusevicius, G. Niaura, Z. Talaikyte, V. Razumas, Vib. Spectrosc. 10 (1996) 271–280.
[38] T. Miura, A. Hori-i, H. Takeuchi, FEBS Lett. 396 (1996) 248–252.
[39] T. Miura, A. Hori-i, H. Mototani, H. Takeuchi, Biochemistry 38 (1999) 11560–11569.
[40] J.K. Beattle, E. Farkas, I. Sóvágó, T. Kiss, J. Chem. Soc. Dalton Trans. (1984) 611–614.
[41] G.F. Bryce, R.W. Roeske, R.N. Gurd, J. Biol. Chem. 241 (1966) 1072–1080.
[42] M.A. Zoroddu, T. Kowalik-Jankowska, H. Kozłowski, H. Molinari, K. Salnikow, L. Broday, M. Costa, Biochim. Biophys. Acta 1475 (2000) 163–168.
[43] W. Bal, M. Diba, F. Kasprzykowski, H. Kozłowski, R. Latajka, L. Lankiewicz, Z. Mackiewicz, L.D. Pettit, Inorg. Chim. Acta 283 (1998) 1–11.
[44] B. Barszcz, J. Kulig, J. Jezierska, J. Lisowski, Pol. J. Chem. 73 (1999) 447–456.
[45] E. Prenesti, P.G. Daniele, M. Prencipe, G. Ostacoli, Polyhedron 18 (1999) 3233–3241.
[46] R.P. Bonomo, G. Impellizzeri, G. Pappalardo, E. Rizzarelli, G. Tabbì, Chem. Eur. J. 6 (2000) 4195–4202.
[47] T. Gajida, B. Henry, S.A. Aubry, J.J. Delpuech, Inorg. Chem. 35 (1996) 586–593.